Applied and Environmental Microbiology, June 2010, p. 3611–3619 Vol. 76, No. 11
0099-2240/10/$12.00 doi:10.1128/AEM.00133-10

Fate of a *Pseudomonas savastanoi* pv. savastanoi Type III Secretion System Mutant in Olive Plants (*Olea europaea* L.)▽†

Isabel Pérez-Martínez,[1]¶§ Luis Rodríguez-Moreno,[1]‡§ Lotte Lambertsen,[1]‖ Isabel M. Matas,[2] Jesús Murillo,[3] Stefania Tegli,[4] Antonio J. Jiménez,[1] and Cayo Ramos[2]*

Departamento de Biología Celular, Genética y Fisiología, Facultad de Ciencias, Universidad de Málaga, Campus de Teatinos s/n, E-29071 Málaga, Spain[1]; Instituto de Hortofruticultura Subtropical y Mediterránea "La Mayora," Universidad de Málaga-Consejo Superior de Investigaciones Científicas, Área de Genética, Facultad de Ciencias, Universidad de Málaga, Campus Teatinos s/n, E-29010 Málaga, Spain[2]; Departamento de Producción Agraria, Universidad Pública de Navarra, Campus de Arrosadía, E-31006 Pamplona, Spain[3]; and Dipartimento di Biotecnologie Agrarie, Universitá degli Studi di Firenze, Sez. Patologia Vegetale, Laboratorio di Patologia Vegetale Molecolare, Via della Lastruccia 10, 50019 Sesto Fiorentino, Italy[4]

Received 19 January 2010/Accepted 26 March 2010

Pseudomonas savastanoi **pv. savastanoi strain NCPPB 3335 is a model bacterial pathogen for studying the molecular basis of disease production in woody hosts. We report the sequencing of the *hrpS*-to-*hrpZ* region of NCPPB 3335, which has allowed us to determine the phylogenetic position of this pathogen with respect to previously sequenced *Pseudomonas syringae hrp* clusters. In addition, we constructed a mutant of NCPPB 3335, termed T3, which carries a deletion from the 3′ end of the *hrpS* gene to the 5′ end of the *hrpZ* operon. Despite its inability to multiply in olive tissues and to induce tumor formation in woody olive plants, *P. savastanoi* pv. savastanoi T3 can induce knot formation on young micropropagated olive plants. However, the necrosis and formation of internal open cavities previously reported in knots induced by the wild-type strain were not observed in those induced by *P. savastanoi* pv. savastanoi T3. Tagging of *P. savastanoi* pv. savastanoi T3 with green fluorescent protein (GFP) allowed real-time monitoring of its behavior on olive plants. In olive plant tissues, the wild-type strain formed aggregates that colonized the intercellular spaces and internal cavities of the hypertrophic knots, while the mutant T3 strain showed a disorganized distribution within the parenchyma of the knot. Ultrastructural analysis of knot sections revealed the release of extensive outer membrane vesicles from the bacterial cell surface of the *P. savastanoi* pv. savastanoi T3 mutant, while the wild-type strain exhibited very few vesicles. This phenomenon has not been described before for any other bacterial phytopathogen during host infection.**

The Gram-negative plant-pathogenic bacterium *Pseudomonas syringae* is an economically important pathogen and a relevant model for the study of plant-microbe interactions (1, 16). Based on its pathogenicity and host range, the species is divided into at least 50 pathovars, of which glycinea, phaseolicola, and savastanoi were transferred to the newly defined species *Pseudomonas savastanoi* (8). In addition, DNA-DNA hybridization and multilocus sequence typing divide the *P. syringae* group, which includes *P. savastanoi* pathovars, into at least nine different genomospecies (9, 35).

Bacteria of the *P. syringae* group cause disease by suppressing plant defense responses after injecting specialized proteins, called effectors, into the host cell cytoplasm using a type III secretion system (T3SS) (12). The *P. syringae* T3SS is encoded by a regulon of approximately 20 genes that are organized into a classic pathogenicity island, called the *hrp* cluster, which is required both for the hypersensitive response (HR) and for pathogenesis (10, 14, 24, 25). A set of these genes have been designated *hrc* genes, because they are involved in the HR and are conserved among a wide range of animal and plant pathogens (2, 7). In addition, sequence analysis of the *hrpS*-to-*hrpB* region, which includes the *hrpZ* operon, has shown that *P. syringae* strains can be divided into five phylogroups (17). In parallel with sequence analyses, genetic dissection of the T3SS regulon has allowed the identification of *hrp* and *hrc* genes that are essential for the pathogenicity of *P. syringae* pathovars that affect herbaceous plants. However, knowledge of the pathogenicity determinants of *P. syringae* and *P. savastanoi* pathovars that are required for infection of woody plants, including those of tumor-inducing strains, lags far behind.

Pseudomonas phytopathogens that induce tumor formation in host plants are restricted to *P. savastanoi* pathovars nerii, retacarpa, and savastanoi. Infection of *Olea europaea* L. by *P. savastanoi* pv. savastanoi leads to hypertrophy of the stems and branches and, occasionally, of the leaves and fruits (19). The

* Corresponding author. Mailing address: Área de Genética, Facultad de Ciencias, Universidad de Málaga, Campus de Teatinos s/n, E-29071 Málaga, Spain. Phone: 34-95213 1955. Fax: 34-95213 2001. E-mail: crr@uma.es.

§ I.P.-M. and L.R.-M. contributed equally to this work.

¶ Present address: Département de Microbiologie Fondamentale (DMF), Quartier UNIL-Sorge, Bâtiment Biophore, CH-1015 Lausanne, Switzerland.

‡ Present address: Centro de Edafología y Biología Aplicada del Segura, Consejo Superior de Investigaciones Científicas, E-30100 Espinardo, Murcia, Spain.

‖ Present address: Department of Bacteriology, Mycology and Parasitology, Statens Serum Institut, DK-2300 Copenhagen S, Denmark.

† Supplemental material for this article may be found at http://aem.asm.org/.

▽ Published ahead of print on 2 April 2010.

first and best-characterized *P. savastanoi* determinants that have been shown to be involved in olive knot development are the phytohormones indoleacetic acid (IAA) and cytokinins (CKs) (11, 31, 32, 41). More recently, it was shown that inactivation of the *hrpC* cluster by insertional mutagenesis of the *hrcC* gene completely abolishes induction of knot formation by *P. savastanoi* pv. savastanoi strain ITM317, despite its intact ability to produce IAA and CKs (38). However, with the exception of the *hrpE* gene and the *hrpC* operon (38), the sequences and roles of the *hrp* and *hrc* genes in the virulence and pathogenicity of tumor-inducing *P. savastanoi* strains have not yet been determined.

P. savastanoi pv. savastanoi strain NCPPB 3335 is a model organism for the study of the pathosystem *P. savastanoi* pv. savastanoi olive because it can accept foreign DNA with a high frequency in comparison to other *P. savastanoi* pv. savastanoi strains (29). In addition, this strain is highly virulent to olive plants, both in adult plants and in young micropropagated plants (32). Furthermore, descriptions of the endopathogenic lifestyle of NCPPB 3335 in olive knots (33) and the genetic contents of its plasmids (30) have been recently reported. However, future studies on the function of *P. savastanoi* pv. savastanoi T3SS effectors, including their translocation into plant cells, require the availability of a T3SS mutant of *P. savastanoi* pv. savastanoi NCPPB 3335 and a broader understanding of the role of the T3SS in the colonization of olive tissues by this pathogen and in the biological processes involved in tumor formation and its development, which was the aim of this study.

MATERIALS AND METHODS

Bacterial strains and growth conditions. *P. savastanoi* pv. savastanoi strains were routinely cultured at 28°C in LB medium (23) that was supplemented, when required, with 100 μg/ml ampicillin (Ap), 10 μg/ml gentamicin (Gm), and 7 μg/ml kanamycin (Km). *P. savastanoi* pv. savastanoi strain NCPPB 3335 was isolated in 1984 from a diseased olive tree in France. A T3SS mutant of this strain, named T3, was constructed as described below. Green fluorescent protein (GFP)-tagged derivatives of NCPPB 3335 and T3 harboring the pLRMl-GFP plasmid (33) are referred to here as NCPPB 3335-GFP (33) and T3-GFP, respectively. Transformation of electrocompetent *P. savastanoi* pv. savastanoi cells with pLRM1-GFP was performed as previously described (29).

General molecular techniques. Agarose gel electrophoresis and other standard recombinant DNA techniques were performed as described previously (34). Genomic DNA was extracted using the Jet Flex Extraction Kit (Genomed, Löhne, Germany) according to the manufacturer's instructions. For Southern blotting, genomic DNA was digested with appropriate restriction enzymes and separated by electrophoresis using 0.8% agarose gels in 1× TBE. The digested DNA was transferred to positively charged nylon membranes (Sigma-Aldrich, Inc., St. Louis, MO) by upward capillary transfer and cross-linked by UV irradiation. DNA fragments from the *aphA* (Km resistance), *hrpS*, *hrpA*, and *hrpZ* genes were amplified by PCR using specific primers (Table 1), labeled individually with a nonradioactive digoxigenin kit (Roche, Mannheim, Germany) according to the manufacturer's instructions, and used as probes. Hybridization was performed at 65°C.

Construction of a T3SS mutant of *P. savastanoi* pv. savastanoi NCPPB 3335 by marker exchange mutagenesis. The pUC18N-Km plasmid (27) is a pUC18Not derivative (15) that carries the SphI fragment of pMKm (26), which contains an *aphA* gene. The PCR fragments for the *hrpS* and *hrpZ* genes were amplified from *P. savastanoi* pv. savastanoi strain NCPPB 3335 using primers designed according to the genetic sequence of its closest relative, *P. syringae* pv. phaseolicola 1448A (18). First, the *hrpS* fragment was cloned into the EcoRI/KpnI-digested pUC18N-Km plasmid, resulting in the formation of the p18N-S-Km plasmid. Then, the *hrpZ* fragment was cloned into the BamHI/XbaI-digested p18N-S-Km plasmid, yielding plasmid p18N-S-Km-Z; the EcoRI-XbaI fragment of this plasmid was then cloned into the pKAS32 plasmid (39), resulting in the formation of the pKAS-S-Km-Z plasmid. The resulting mutagenic DNA contained a deletion of the last 8 amino acids of *hrpS* and the whole coding sequence of *hrpA*, also including the *hrp* box preceding *hrpA*, which likely controls the expression of the *hrpZ* operon. For marker exchange mutagenesis, the pKAS-S-Km-Z plasmid was introduced into the recipient strain *P. savastanoi* pv. savastanoi NCPPB 3335 by biparental mating (29) using *Escherichia coli* S17-1 (37) as the donor strain.

TABLE 1. Oligonucleotide primers used in this work

Name	Primer sequence (5′–3′)[a]	Reference
HrpA-F	CGCTGGAACCGATTTAAGGG	This study
HrpA-R	CACAACCTCCTCAAAGTAGCAG	This study
HrpS-F	TGAATTCGAGGAGCGTGTTCCA AATCTG; EcoRI	This study
HrpS-R	TTGGTACCATAGAGCGTGCGG CGTGG; KpnI	This study
HrpZ-F	TGGATCCGGCTGCTACTTTGAG GAGGTTG; BamHI	This study
HrpZ-R	TATCTAGAGGTCACTTGAGTTC TCCGTCAG; XbaI	This study
Km-*aphA*-R	ATGAGCCATATTCAACGG	29
Km-*aphA*-F	AGCATCAAATGAAACTGC	29

[a] Underlined bases represent restriction sites (shown to the right of the sequence) introduced for cloning of PCR-amplified fragments.

DNA sequencing. A 2,422-bp fragment containing a partial *hrpS* open reading frame (ORF), the intergenic region located between *hrpS* and *hrpA*, and the complete *hrpA* and *hrpZ* ORFs was amplified from *P. savastanoi* pv. savastanoi NCPPB 3335 using primers HrpS-F and HrpZ-R (Table 1). After amplification, the fragment was sequenced using the ABI Prism BigDye Terminator Ready Reaction Kit V 3.1 and the 3730 DNA Analyzer (both from Applied Biosystems).

Phylogenetic analysis. Multiple-sequence alignment of the DNA and amino acid sequences was performed using Clustal W version 1.8 software (45). Neighbor-joining (NJ) trees were generated with 10,000 bootstrap replicates for all sequences using MEGA4 (43). The DNA sequences of the *hrpS*, *hrpA*, and *hrpZ* genes of the *P. syringae* strains used for phylogenetic analysis were downloaded from the GenBank database, and their accession numbers are shown in Table S1 in the supplemental material. Cluster analysis of the amino acid sequences of HrpS, HrpA, and HrpZ was performed as previously described (17). For analysis of the sequences of HrpS putative proteins, the C-terminal 159 amino acid residues of these proteins were used.

Plant infection and isolation of bacteria from olive knots. Olive plants (*Olea europaea* L.) derived from seeds germinated *in vitro* (originally collected from a cv. Arbequina plant) were micropropagated and rooted, as previously described (32), in Driver Kuniyuki Walnut (DKW) medium (4). Rooted explants were transferred to DKW medium without hormones and kept for at least 2 weeks in a growth chamber at 25 ± 1°C with a 16-h photoperiod prior to infection. The olive plants used for *in vitro* studies were 60 to 80 mm long (stem diameter, 1 to 2 mm) and contained three to five internodal fragments.

Micropropagated olive plants were wounded by excision of an intermediate leaf and infected in the stem wound with a bacterial suspension under sterile conditions. For this purpose, bacterial lawns were grown for 48 h in LB plates and resuspended in 10 mM $MgCl_2$. The concentration of the bacterial cells was adjusted to an optical density at 600 nm (OD_{600}) of 0.1, corresponding to 10^7 CFU/ml. The plant wounds were infected with two microliters (approximately 10^4 CFU) of the resulting cell suspension. The plants were then incubated in a growth chamber at 25 ± 1°C with a 16-h photoperiod and a light intensity of 35 μmol × m^2/s. At different time points, *P. savastanoi* pv. savastanoi cells were recovered from the infected explants and spotted onto LB (to detect NCPPB 3335) or LB-Gm (to detect NCPPB 3335-GFP and T3-GFP) plates as previously described (33). Population densities were calculated from at least three replicates. The morphology of the olive plants infected with bacteria was visualized using a stereoscopic microscope (Leica MZ FLIII).

To analyze the pathogenicity of *P. savastanoi* pv. savastanoi isolates in 1-year-old olive explants, micropropagated olive plants were transferred to soil and maintained in a greenhouse at 27°C with a relative humidity of 58% under natural daylight. The plants were wounded at five sites on the main stem. The wounds, which were 0.5 cm deep and spanned from the stem surface to the cambial area, were made with a sterile scalpel. Each wound was infected with approximately 10^6 CFU of *P. savastanoi* pv. savastanoi strains. For this purpose, bacterial suspensions were prepared as previously described (28, 29). Morphological changes, scored 90 days after infection, were captured with a high-

resolution digital camera (Nikon DXM 1200), and the images were processed using Adobe Photoshop CS software.

Hypersensitive response assays. *Nicotiana tabacum* var. Newdel plants were grown at 23/26°C with a photoperiod cycle of 16/8 h of light/dark and a light intensity of 40 μmol × m^2/s. Bacterial cells of the corresponding strain were grown overnight in LB medium at 28°C, resuspended in 10 mM $MgCl_2$, and adjusted to an OD_{600} of 0.5, which corresponds to approximately 5×10^7 CFU/ml. Three tobacco plants were infected per strain in the intracellular spaces of the abaxial side of a leaf with 100 to 200 μl of bacterial suspension (approximately 10^7 CFU). Penetration of the bacterial suspension into the intracellular leaf space was achieved by pressing a 2-ml syringe without a needle to the underside of the leaf. The development of HR was scored 24 h after infection. Symptoms were captured with a high-resolution digital camera (Nikon DXM 1200), and the images were processed using Adobe Photoshop CS software.

Real-time monitoring of bacterial infection by epifluorescence microscopy and scanning confocal electron microscopy (SCEM). To visualize bacterial infection within tumors in real time, whole knots were directly examined with a stereoscopic fluorescence microscope (Leica MZ FLIII) equipped with a 100-W mercury lamp and a GFP2 filter (excitation, 480/40 nm). Images were captured using a high-resolution digital camera (Nikon DXM 1200), and the images were processed using Adobe Photoshop CS software.

To visualize bacterial infection within the tumors of the olive plants, the knots were sampled on different days postinoculation (p.i.) at locations 1 cm above and 1 cm below the inoculation point. These samples were fixed and embedded in agarose as previously described (33). Samples were fixed overnight at 4°C in 2.5% paraformaldehyde (PFA) prepared in 0.1 M phosphate buffer, pH 7.4. The fixed samples were then transferred into 2.5% PFA with an ascending gradient of 10%, 20%, and 30% sucrose for 10, 20, and 30 min, respectively. Finally, samples were embedded in 7% low-melting-point agarose and cooled to 4°C. Sections (40 and 60 μm thick) were cut from the knot samples using a freezing microtome (Leica CM1325). Fluorescence of the bacterial cells within knot sections was visualized by epifluorescence microscopy using a Nikon Microphot FXA microscope. For confocal microscopy, we used an inverted SCEM (model TCS-NT; Leica, Germany) equipped with detectors and filters that simultaneously detect green and red fluorescence. Images of green fluorescence were acquired at an excitation wavelength of 488 nm and an emission wavelength of 500 to 560 nm. The images were acquired by sequential scan analysis and processed using Adobe PhotoShop 6 software (Adobe, Mountain View, CA).

Transmission electron microscopy (TEM). Cross sections (1 to 2 mm thick) were cut from the fixed knots using a blade. The sections were then immersed in a solution of 3% glutaraldehyde and 0.1 M cacodylate buffer (pH 7.4) for 2 h at room temperature and then at 4°C overnight. Postfixation was performed in cold 1% osmium tetroxide, prepared in 0.1 M cacodylate buffer, for 2 h at 4°C. The fixed sections were then dehydrated and embedded in Araldite 502 (EMS, Hatfield, PA). Semithin (1-μm-thick) and ultrathin (50- to 70-nm-thick) sections of the knots were cut using an ultramicrotome (Ultracut E; Leica, Germany). The semithin sections were mounted on glass slides and stained with 1% toluidine blue. The ultrathin sections were mounted on grids, stained with Reynold's lead citrate solution and uranyl acetate, and visualized using a Philips CM100 electron microscope.

Nucleotide sequence accession number. The sequence of the 2,422-bp fragment containing a partial *hrpS* ORF, the intergenic region located between *hrpS* and *hrpA*, and the complete *hrpA* and *hrpZ* ORFs was deposited in GenBank under accession number GU299771.

RESULTS

Sequence analysis of *P. savastanoi* pv. savastanoi NCPPB 3335 *hrpS*, *hrpA*, and *hrpZ* genes. A 2,422-bp fragment containing a partial *hrpS* ORF, the intergenic region located between *hrpS* and *hrpA*, and the complete *hrpA* and *hrpZ* ORFs was amplified from *P. savastanoi* pv. savastanoi NCPPB 3335 and sequenced as described in Materials and Methods. Analysis of this fragment revealed a 98% nucleotide identity to the corresponding *P. syringae* pv. phaseolicola 1448A sequence (18). The deduced amino acid sequences of the NCPPB 3335 HrpS, HrpA, and HrpZ proteins showed 99%, 97%, and 96% identity, respectively, with the corresponding *P. syringae* pv. phaseolicola 1448A sequences.

Cluster analysis of the HrpS sequences revealed that *P. savastanoi* pv. savastanoi NCPPB 3335 belongs to group I of the HrpS proteins (see Fig. S1A in the supplemental material), which is comprised exclusively of proteins from *P. syringae* pathovars that belong to genomospecies 2 (9), such as phaseolicola, glycinea, sesami, morsprunorum, tabaci, and lachrymans.

In the cluster analysis based on the sequence of HrpA, *P. savastanoi* pv. savastanoi NCPPB 3335 was classified into group IA of division 1 (17). Thus, this strain contains an *hrpA2* gene that encodes a 108-amino-acid protein that is highly similar to those of *P. syringae* pathovars phaseolicola (1448A), glycinea (race 0), and tabaci (strain 11528) (see Fig. S1B in the supplemental material). Cluster analysis of the sequences of HrpZ also classified *P. savastanoi* pv. savastanoi NCPPB 3335 in the same group of strains (see Fig. S1C in the supplemental material).

Sequence analysis of the intergenic region located between *hrpS* and *hrpA* revealed the existence of a sequence (GGAA CCG-N_{15}-CCACCTA) that matched the HrpL-dependent promoter consensus sequence, or Hrp box, of *P. syringae* (6). Multialignment of this 29-base fragment with the corresponding DNA fragments of previously sequenced *P. syringae* strains revealed that all of them share an identical Hrp box, independent of the type of HrpA protein encoded by each strain. Furthermore, the 15-base sequence (N_{15}) located between the two conserved motifs in this putative Hrp box of *P. savastanoi* pv. savastanoi NCPPB 3335 was identical to those of *P. syringae* pathovars phaseolicola, glycinea, and tabaci (see Fig. S2 in the supplemental material).

Genetic characterization of *P. savastanoi* pv. savastanoi T3, a T3SS mutant derived from NCPPB 3335. For marker exchange mutagenesis, the pKAS-S-Km-Z suicide plasmid was introduced into recipient strain *P. savastanoi* pv. savastanoi NCPPB 3335. Transconjugants were selected on LB medium containing Km, and replica plates of the resulting colonies were made on LB-Ap plates to determine whether each transconjugant underwent plasmid integration (Ap^r) or allelic exchange (Ap^s). A Km^r Ap^s strain called T3 was selected and further characterized. To verify that double homologous recombination between the pKAS-S-Km-Z plasmid and the genome of NCPPB 3335 resulted in *aphA* disruption of the *hrpA* ORF (Fig. 1A), EcoRI-digested total DNA isolated from both *P. savastanoi* pv. savastanoi T3 and NCPPB 3335 was hybridized with *aphA*, *hrpA*, *hrpS*, and *hrpZ* probes. The *aphA* probe did not hybridize with the NCPPB 3335 sample. In contrast, a single hybridization band was obtained for T3 using this probe. The *hrpA* probe hybridized only with the wild-type strain NCPPB 3335, yielding a single hybridization band. These results were expected, since neither the *aphA* ORF nor the DNA fragment spanning from *hrpS* to *hrpZ*, which also includes *hrpA*, contains EcoRI sites. Furthermore, hybridization with *hrpS* and *hrpZ* probes yielded a single band with both NCPPB 3335 and T3 strains; however, the size of the hybridization band obtained for T3 was larger than that of the wild-type strain. This result was expected, since the *hrpA* ORF and the intergenic region located between *hrpS* and *hrpA* were replaced by the *aphA* cassette (Fig. 1). Disruption of this DNA region in *P. savastanoi* pv. savastanoi T3 was further confirmed by PCR and sequencing (data not shown).

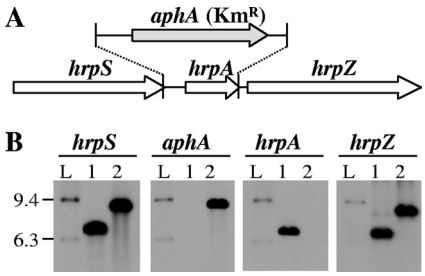

FIG. 1. (A) Schematic representation of the organization of the *hrpS*, *hrpA*, and *hrpZ* genes in *P. savastanoi* pv. savastanoi NCPPB 3335. *P. savastanoi* pv. savastanoi T3 carries an *aphA* disruption covering from the 3′ end of the *hrpS* gene to the 5′ end of the *hrpZ* operon. (B) Southern blot analysis of EcoRI-digested genomic DNA isolated from NCPPB 3335 (lanes 1) and T3 (lanes 2). The DNA probes used are indicated above each image. Lanes L, HindIII-digested λ phage DNA. The positions of the molecular size markers (in kilobases) are indicated on the left of the gel.

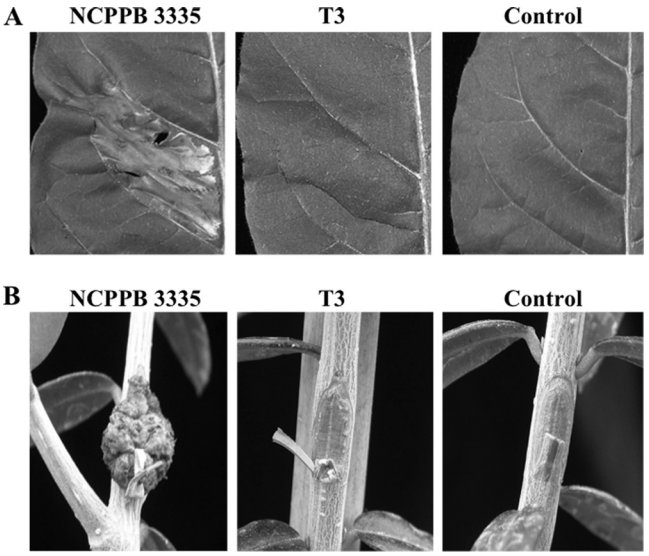

FIG. 2. (A) Hypersensitive response on *N. tabacum* leaves 24 h after infection with *P. savastanoi* pv. savastanoi NCPPB 3335 or T3SS mutant T3. (B) Symptoms induced on the stems of 1-year-old olive plants 90 days after inoculation with NCPPB 3335 or T3. Control, treatments with 10 mM $MgCl_2$.

***P. savastanoi* pv. savastanoi T3 induces knot formation on young micropropagated olive plants, but not in woody plants.** As expected for a *P. savastanoi* pv. savastanoi strain, NCPPB 3335 elicited a characteristic HR in tobacco leaves 24 h after infiltration; however, T3 did not induce this incompatible reaction (Fig. 2A). Thus, induction of HR by *P. savastanoi* pv. savastanoi NCPPB 3335 in tobacco leaves depends on a functional T3SS. The pathogenicity of *P. savastanoi* pv. savastanoi T3 was first examined in 1-year-old olive plants and compared to the pathogenicity of the wild-type strain. In agreement with previous reports (29), the wild-type strain induced visible knots on the stems of the olive plants at 90 days p.i., whereas *P. savastanoi* pv. savastanoi T3 did not. The appearance of the stems infected with the mutant strain was identical to that of control plants inoculated with a solution of $MgCl_2$ (Fig. 2B). Thus, a functional *P. savastanoi* pv. savastanoi *hrpZ* operon seems to also be required for knot formation in woody olive plants.

Recently, we reported the construction of a *P. savastanoi* pv. savastanoi strain carrying a stable plasmid vector expressing GFP (pLRM1-GFP) in combination with the use of young micropropagated olive plants, which are highly susceptible to knot formation. In this system, the time required for symptoms to occur is significantly reduced in comparison to older plants, and it allows real-time monitoring of *P. savastanoi* pv. savastanoi infection (32, 33). The ability of *P. savastanoi* pv. savastanoi T3 to grow in olive plant tissues was markedly reduced in comparison to the wild-type strain. NCPPB 3335 multiplied in the olive tissues within 1 week when the plants were infected with a diluted suspension (approximately 10^4 to 10^5 CFU), reaching approximately 10^7 CFU at 7 days p.i. Thereafter, bacterial counts for the strain remained at this level throughout the duration of the experiment (28 days p.i.). In contrast, the population sizes of *P. savastanoi* pv. savastanoi T3 and its GFP-tagged derivative remained at 10^4 to 10^5 CFU until the end of the experiment (Fig. 3A).

Despite the low cell density observed for *P. savastanoi* pv. savastanoi T3 in olive plants, swelling of the stem tissues was visualized at 5 days p.i. in plants infected with either the wild-type or the mutant strain; this response was followed by knot formation, which was visible at 9 days p.i. Similar results were obtained after infection with NCPPB 3335-GFP and T3-GFP. The size of the knots increased from 9 to 28 days p.i. in plants infected with each of these four strains. However, the wild-type strain and its GFP derivative exhibited necrotic lesions covering the hypertrophic tissue at 28 days p.i. In contrast, T3-GFP-induced tumors lacked such lesions (Fig. 3B). In general, the tumors induced by the mutant strain were whiter than those induced by the wild-type strain (Fig. 3B). Thus, the induction of necrosis previously reported in knots produced by wild-type NCPPB 3335 in young micropropagated olive plants (33) is dependent on a functional T3SS.

As we previously reported (33), we were able to monitor *P. savastanoi* pv. savastanoi infection in real time using epifluorescence microscopy in plants infected with NCPPB 3335-GFP. The knots induced by this strain exhibited green fluorescent clusters that spanned the entire surface of the knot at 28 days p.i. However, plants infected with mutant T3-GFP exhibited only small nuclei of green fluorescence, which were restricted to the stem wounds infected with bacteria, at 5 and 9 days p.i.. Beyond this time point, the green fluorescence detected in the knots could not be distinguished from the autofluorescence detected in control plants infected with the nonfluorescent wild-type bacteria (Fig. 3C).

Knots induced by *P. savastanoi* pv. savastanoi T3 on young micropropagated olive plants show neither aggregation of pathogen cells nor lysis of host cells. The knots induced by NCPPB 3335-GFP on young micropropagated olive plants exhibit histological features similar to those previously reported in older olive plants, such as hypertrophic parenchymal tissue that expands from the vascular cylinder and exhibits internal open fissures surrounded by plasmolyzed cells (33). The localization of GFP-tagged bacterial cells in knot tissues was monitored by epifluorescence and SCEM. The autofluorescence

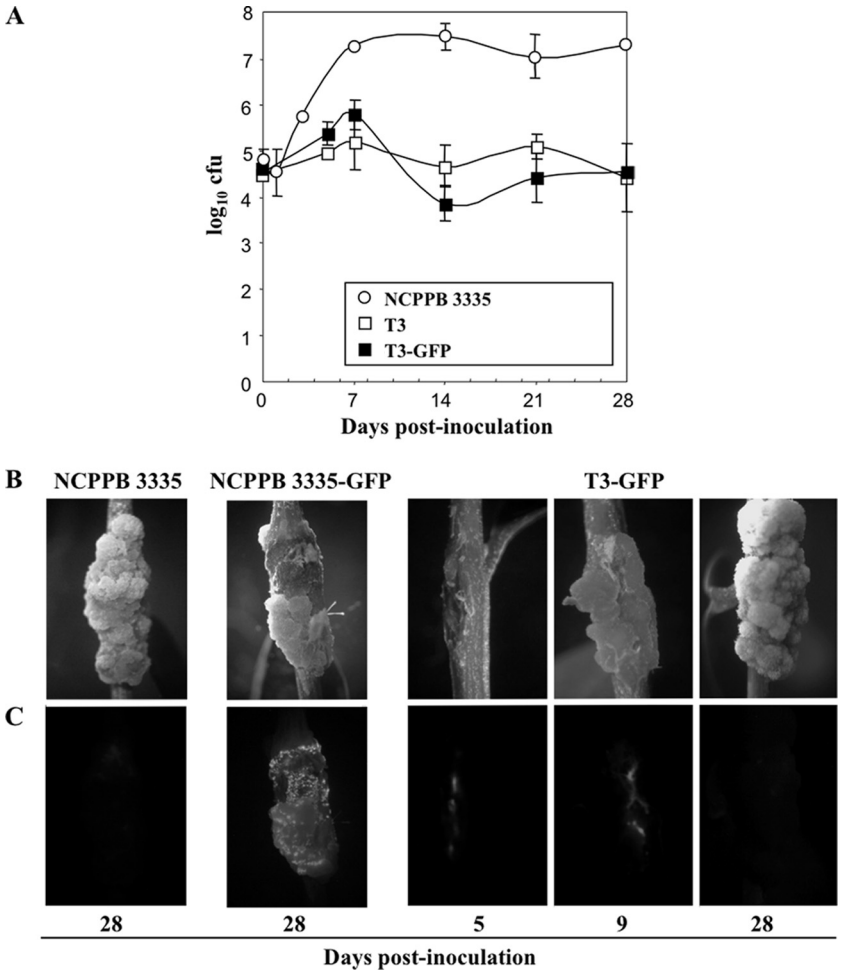

FIG. 3. (A) Growth curves of NCPPB 3335 (○), T3 (□), and T3-GFP (■) strains in young micropropagated olive plants. The data represent the averages of three independent experiments; the error bars indicate the standard deviations from the averages. (B) Images of knots induced by *P. savastanoi* pv. savastanoi strains NCPPB 3335, NCPPB 3335-GFP, and T3-GFP on olive plants. (C) Complementary epifluorescence microscopy images of knots induced by the indicated strains.

emitted by the plant tissues was used to differentiate the histological structures found in the knot sections (33). Transverse sections of the knots induced by NCPPB 3335-GFP at 28 days p.i. clearly showed expanded areas of green fluorescent spots colonizing the internal open cavities and periphery of the knot tissues (Fig. 4A). In contrast, only a few small spots of GFP-tagged cells were visualized near the main vascular cylinder of the knots induced by T3-GFP at 28 days p.i. (Fig. 4B). Interestingly, the internal cavities observed in the sections of the knots induced by the GFP-tagged wild-type strain (Fig. 4A) were not evident in those induced by the T3SS mutant (Fig. 4B). To view the parenchymal tissues of the olive plant knots in more detail, transverse semithin sections of the knots induced at 35 days p.i. by NCPPB 3335-GFP and T3-GFP were stained with toluidine blue and visualized by light microscopy. The characteristic internal cavities formed in knots induced by the GFP-tagged wild-type strain are shown in Fig. 4C and E. In contrast, tumors induced by T3-GFP exhibited a compact tissue structure composed of parenchyma-like cells (Fig. 4D) and newly formed nuclei of xylem and phloem vessels (Fig. 4F); these structures were also visualized in the knots induced by the wild-type strain (33). However, the plasmolyzed host cells surrounding the internal open cavities were not observed in the hypertrophic tissue of the knots induced by the T3SS mutant. Thus, lysis of host cells within the knots induced by *P. savastanoi* pv. savastanoi on young micropropagated olive plants is dependent on a functional T3SS.

High-magnification images of knot sections induced at 28 days p.i. by NCPPB 3335-GFP and T3-GFP were analyzed by SCEM. Aggregates of NCPPB 3335-GFP cells were observed filling the intercellular spaces of the parenchymal tissues and colonizing the cell surfaces and internal cavities of the knots (Fig. 4G). These aggregates are composed of multilayer biofilms, and their visualization by scanning electron microscopy (SEM) has been previously reported (33). T3-GFP cells, in contrast, exhibited a disorganized distribution within the parenchymal knot tissues (Fig. 4H).

Ultrastructural analysis of *P. savastanoi* pv. savastanoi T3-induced knots on young micropropagated olive plants. Ultrathin sections of olive plant knots induced by *P. savastanoi* pv. savastanoi T3 at 35 days p.i. were analyzed by TEM and compared with knots induced by the wild-type strain. The ultra-

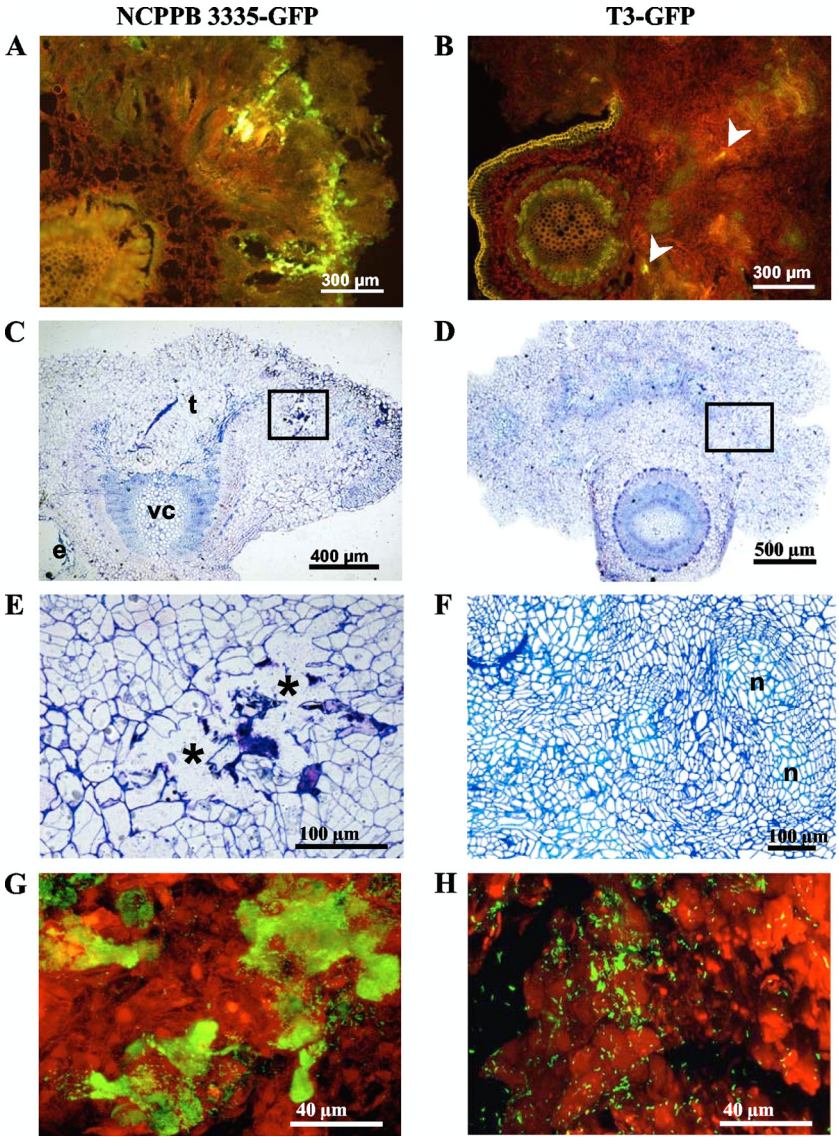

FIG. 4. Microscopic analysis of knots induced by *P. savastanoi* pv. savastanoi NCPPB 3335-GFP (A, C, E, and G) and T3-GFP (B, D, F, and H) on young micropropagated olive plants. (A and B) Epifluorescence microscopy images of transverse sections of knots induced by NCPPB 3335-GFP and T3-GFP, respectively, 28 days p.i. (C, D, E, and F) Light microscopy images of semithin cross sections of knots stained with toluidine blue. (C and D) Panoramic view of knots induced by NCPPB 3335-GFP and T3-GFP, respectively, 35 days p.i. e, epidermis; vc, vascular cylinder; t, hypertrophied parenchyma. (E) Detail of boxed area in panel C showing characteristic open fissures (asterisks) surrounded by disorganized and collapsed parenchymal cells. (F) Detail of boxed area of panel D showing compacted hypertrophic tissue containing newly formed nuclei of xylem vessels (n). (G and H) Scanning confocal laser microscopy images of knots induced by NCPPB 3335-GFP and T3-GFP, respectively, at 28 days p.i.

structure of the olive plant knots induced by the wild-type strain (Fig. 5A and B) was identical to that previously reported for its GFP-tagged derivative (33). Also in agreement with this report, we found that outer membrane vesicles (OMVs) were released from the cell surface of the wild-type strain (Fig. 5B). In contrast, *P. savastanoi* pv. savastanoi T3 cells exhibited an irregular morphology and were localized only to the intercellular spaces of parenchyma-like cells (Fig. 5C and D). Host cells in contact with either the wild-type (Fig. 5A) or the mutant (Fig. 5C) strain exhibited a degenerated cytoplasm and electron-lucent points surrounded by secondary cell wall depositions. Interestingly, high-magnification images of *P. savastanoi* pv. savastanoi T3 cells, which were surrounded by an electron-lucent halo and immersed in a fibroreticular matrix, clearly showed that a significant number of vesicles emerged from the outer membrane of the bacterial envelope and fused with the fibroreticular matrix (Fig. 5D). The release of these OMVs was drastically enhanced in the mutant strain (Fig. 5D) compared to the wild-type strain (Fig. 5B).

DISCUSSION

P. savastanoi pv. savastanoi is an unusual member of the *P. syringae* group in that it induces the formation of aerial tumors

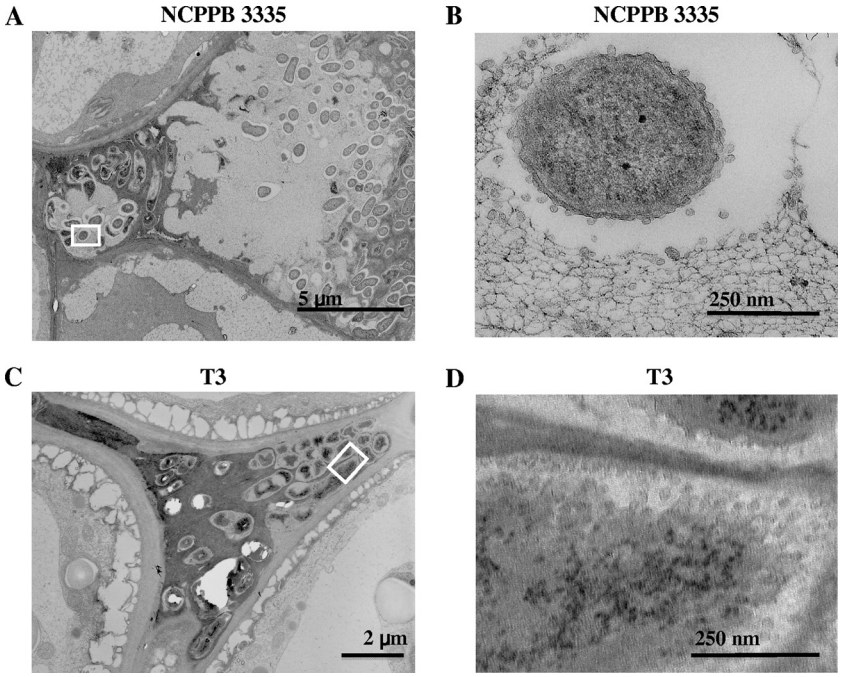

FIG. 5. Transmission electron micrographs of ultrathin sections of knots induced by *P. savastanoi* pv. savastanoi NCPPB 3335 (A and B) and T3 (C and D) at 35 days p.i. on olive plants. (A) Ultrastructure of the parenchymal knot tissue invaded by rod-shaped wild-type bacteria. (C) Intercellular space located between parenchyma-like cells filled with *P. savastanoi* pv. savastanoi T3 cells showing abnormal morphology. (B and D) Details of the boxed areas in panels A and C, respectively, showing the release of OMVs from the cell surfaces of the indicated bacterial strains.

in a woody plant host. Symptom development on olive plants has been associated with the ability of the bacterium to produce phytohormones that alter the physiological hormone balance in infected tissues (19). In contrast with the tumor-inducing bacteria *Agrobacterium tumefaciens* and *Rhodococcus fascians*, *P. savastanoi* pv. savastanoi is endowed with a T3SS, which is also required for knot formation in woody olive plants (38), and a corresponding set of T3SS effectors (30). The *P. syringae hrpZ* operon encodes the pore-forming hairpin HrpZ; the pilus subunit HrpA; the conserved HrcJ protein, which is associated with the inner and outer bacterial membranes; and the HrpB, HrpD, and HrpE proteins, whose functions are unknown. Therefore, this operon is an excellent genetic element for the study of the evolutionary forces that drive host-pathogen interactions (13). The results of our sequence analysis of the NCPPB 3335 *hrpS*, *hrpA*, and *hrpZ* genes supports the previous hypothesis that the genetic composition, arrangement, and operon organization of the *hrp-hrc* gene cluster of *P. savastanoi* resembles that of *P. syringae* (38). In addition, it allowed us to classify *P. savastanoi* pv. savastanoi within the previously defined *hrp* phylogroups of *P. syringae* (13, 17) and to group *P. savastanoi* pv. savastanoi NCPPB 3335 with other *P. syringae* pathovars that are included in genomospecies 2 (see Fig. S1 in the supplemental material). These results are in agreement with previous phylogenetic studies of the *P. syringae* group based on housekeeping genes (36) and suggest that the current nomenclature for these bacteria needs to be carefully revised because their taxonomy and phylogeny show marked disparity.

Despite the hypervariability in the amino acid sequences of HrpA proteins from the different pathovars belonging to the *P. syringae* group, our sequence analysis showed that they all have identical *hrp* boxes (see Fig. S2 in the supplemental material) and all have a highly conserved region located between the promoter and the *hrpA* start codon (data not shown). These results suggest that the evolutionary forces acting on *hrpA*, which favor the maintenance of genetic diversity and apparently enable the bacterium to avoid recognition by the host (13), affect neither its transcriptional regulation nor the stability of its mRNA. In *P. syringae* pv. tomato DC3000, the stability of the mRNA has been shown to be dependent on its 5′ nucleotide sequence (42).

As previously reported for a *P. savastanoi* pv. savastanoi ITM317 mutant containing a transposon insertion in gene *hrcC* (38), *P. savastanoi* pv. savastanoi T3 (Fig. 1) could not multiply in olive plant tissues (Fig. 3A), induce HR in tobacco plants (Fig. 2A), or induce tumor formation in woody olive plants (Fig. 2B). In contrast, this mutant strain was capable of inducing knot formation on young micropropagated olive plants (Fig. 3B). In addition, the weights of overgrowths developed on plants infected with *P. savastanoi* pv. savastanoi T3 were not significantly different from the weights of those infected with the parental strain (data not shown). This result is likely due to the high susceptibility of the micropropagated plant material to *P. savastanoi* pv. savastanoi (32) and to the ability of *P. savastanoi* pv. savastanoi T3 to produce IAA. Micropropagated cranberry plants have also been reported to be more susceptible than woody plants to infection with IAA-producing bacteria (46). In agreement with this hypothesis, the wild-type strain and *P. savastanoi* pv. savastanoi T3 produced equal

amounts of IAA in culture medium, as determined by a colorimetric assay (data not shown). In fact, differentiation of parenchymal cells into xylem and phloem vessels, a phenomenon associated with bacterial secretion of phytohormones into the plant tissues (22), has been previously observed in knots induced by the wild-type strain (33) and was shown to be induced by *P. savastanoi* pv. savastanoi T3 on olive plants (Fig. 4F). Our results therefore suggest that the process of tumor formation on young micropropagated olive plants is independent of the T3SS apparatus.

The bacterial aggregates formed in knots from plants infected with NCPPB 3335-GFP (Fig. 4A and G) have been shown to consist of microcolonies of rod-shaped bacteria and multilayer biofilms that colonize the surfaces and interiors of plasmolyzed host cells (33). The low cell density observed for *P. savastanoi* pv. savastanoi T3 in olive plant tissues (Fig. 3A) was consistent with the decreased GFP fluorescence detected in knots induced by T3-GFP in olive plants (Fig. 3C). In addition, we found that the mutant strain lacked the ability to form cell aggregates within olive plant tissues (Fig. 4B and H). Taken together, our results suggest that mutations in the T3SS of *P. savastanoi* pv. savastanoi affect bacterial fitness inside olive knot tissues. Similar results have been reported with respect to the epiphytic and endophytic multiplication of an *hrpA* mutant of *P. syringae* pv. tomato DC3000 in tomato leaves (3). Nevertheless, although the Hrp pili of *P. syringae* and *Dickeya dadantii* (formerly *Erwinia chrysanthemi*) appear to be directly involved in bacterial attachment to plant cells and in the formation of multicellular aggregates *in vitro* (42, 47), their roles in biofilm formation *in planta* have not been reported to date.

The absence of superficial necrosis in knots induced by *P. savastanoi* pv. savastanoi T3-GFP on olive plants (Fig. 3B) was consistent with the integrity of the hypertrophic knot tissue observed (Fig. 4B, D, and F). Thus, the reduced fitness of *P. savastanoi* pv. savastanoi T3, which is associated with the lack of a functional T3SS, seems to prevent the bacterial activity that is required for host cell lysis. Consequently, *P. savastanoi* pv. savastanoi T3 did not colonize the characteristic internal cavities formed by natural isolates of *P. savastanoi* pv. savastanoi in woody plants (40, 44) and young micropropagated olive plants (33). All these results suggest that the *P. savastanoi* pv. savastanoi T3SS is not necessary for hyperplasia of the olive tissue; however, necrosis of the hyperplastic tissue seems to be a T3SS-dependent phenomenon.

The release of outer membrane vesicles from the envelope of NCPPB 3335-GFP cells during colonization of olive knots has been previously reported (33). However, to demonstrate that OMV release by this bacterial strain was not a consequence of GFP expression, ultrastructural analysis of the nontagged wild-type strain was needed. As shown in Fig. 5, the release of OMVs from the cell surface of nontagged NCPPB 3335 is similar to that previously reported for the GFP-tagged strain. Furthermore, the release of these vesicles from the envelope of *P. savastanoi* pv. savastanoi T3 cells found within olive plant tissues was clearly enhanced in comparison with the wild-type strain (Fig. 5). OMVs were always visualized surrounding bacterial cells, and they were never observed either deep in the neighbor network of extracellular matrix or emerging from the plant cell wall (Fig. 5B). Thus, it is very unlikely that the plant cells release these vesicles. The formation of blebs on the surfaces of *P. syringae* pv. phaseolicola cells has been previously observed during its colonization in a nonhost plant. This reaction was postulated to be a consequence of the osmotic shock undergone by the bacteria in the apoplast. Interestingly, formation of these bladder-like structures *in planta* was enhanced by an *hrp* mutant strain, while the wild-type strain exhibited little surface blebbing (5). Bacterial release of OMVs, which is a phenomenon that occurs and is well studied in Gram-negative animal pathogens, plays a role in establishing a colonization niche, carrying and transmitting virulence factors into host cells, and modulating host defenses and responses (20). To the best of our knowledge, no reports exist describing OMV release in bacterial phytopathogens during plant infection. In addition to their roles in promoting virulence, production of OMVs by Gram-negative bacteria has been recently shown to function in the alleviation of bacterial stress (21). In agreement with this study, we found that *P. savastanoi* pv. savastanoi T3 exhibits an abnormal morphology when inside olive plant tissues (Fig. 5C and D). This morphological feature is likely reflective of the stress which *P. savastanoi* pv. savastanoi T3 cells undergo *in planta*. However, further studies will be needed to understand these biological processes in bacterial phytopathogens.

ACKNOWLEDGMENTS

This research has been supported by Spanish Plan Nacional I+D+I grants AGL2008-55311-CO2-01 and AGL2008-55311-CO2-02, cofinanced by FEDER, as well as by Integrated Action Spain-Italy HI01-81 and by Ente Cassa di Risparmio di Firenze (2007.1005 and 2008.1573). I.P.-M. was awarded a Spanish MEC fellowship (AP2002-3800), and L.L. and I.M.M. were supported by Carlsberg Foundation (Denmark) grant ANS-1282/20 and the Ramón Areces Foundation (Spain), respectively.

We thank D. Navas for assistance with confocal microscopy, as well as G. Martín and A. Martínez for help with transmission electron microscopy. A. Rivera and M. Reina are thanked for help with the preparation of olive knot samples for epifluorescence microscopy. We are grateful to E. Santilli for her contribution to the construction of strain *P. savastanoi* pv. savastanoi T3 and to M. Duarte for excellent technical assistance. A. Barceló and I. Vidoy are thanked for the micropropagation of olive plants.

REFERENCES

1. **Agrios, G. N. (ed.).** 2005. Plant pathology, 5th ed. Elsevier Academic Press, San Diego, CA.
2. **Bogdanove, A. J., S. V. Beer, U. Bonas, C. A. Boucher, A. Collmer, D. L. Coplin, G. R. Cornelis, H. C. Huang, S. W. Hutcheson, N. J. Panopoulos, and F. VanGijsegem.** 1996. Unified nomenclature for broadly conserved *hrp* genes of phytopathogenic bacteria. Mol. Microbiol. **20:**681–683.
3. **Boureau, T., J. Routtu, E. Roine, S. Taira, and M. Romantschuk.** 2002. Localization of *hrpA*-induced *Pseudomonas syringae* pv. tomato DC3000 in infected tomato leaves. Mol. Plant Pathol. **3:**451–460.
4. **Driver, J. A., and A. H. Kuniyuki.** 1984. *In vitro* propagation of Paradox walnut rootstock. Hortscience **19:**507–509.
5. **Fett, W. F., and S. B. Jones.** 1995. Microscopy of the interaction of *hrp* mutants of *Pseudomonas syringae* pv. phaseolicola with a nonhost plant. Plant Sci. **107:**27–39.
6. **Fouts, D. E., R. B. Abramovitch, J. R. Alfano, A. M. Baldo, C. R. Buell, S. Cartinhour, A. K. Chatterjee, M. D'Ascenzo, M. L. Gwinn, S. G. Lazarowitz, N. C. Lin, G. B. Martin, A. H. Rehm, D. J. Schneider, K. van Dijk, X. Y. Tang, and A. Collmer.** 2002. Genomewide identification of *Pseudomonas syringae* pv. tomato DC3000 promoters controlled by the HrpL alternative sigma factor. Proc. Natl. Acad. Sci. U. S. A. **99:**2275–2280.
7. **Galán, J. E., and A. Collmer.** 1999. Type III secretion machines: bacterial devices for protein delivery into host cells. Science **284:**1322–1328.
8. **Gardan, L., C. Bollet, M. Abughorrah, F. Grimont, and P. A. D. Grimont.** 1992. DNA relatedness among the pathovar strains of *Pseudomonas syringae* subsp. savastanoi Janse (1982) and proposal of *Pseudomonas savastanoi* sp. nov. Int. J. Syst. Bacteriol. **42:**606–612.

9. **Gardan, L., H. Shafik, S. Belouin, R. Broch, F. Grimont, and P. A. D. Grimont.** 1999. DNA relatedness among the pathovars of *Pseudomonas syringae* and description of *Pseudomonas tremae* sp. nov. and *Pseudomonas cannabina* sp. nov. (ex Sutic and Dowson 1959). Int. J. Syst. Bacteriol. **49:**469–478.
10. **Gilchrist, D. G.** 1998. Programmed cell death in plant disease: the purpose and promise of cellular suicide. Annu. Rev. Phytopathol. **36:**393–414.
11. **Glass, N. L., and T. Kosuge.** 1988. Role of indoleacetic acid lysine synthetase in regulation of indoleacetic-acid pool size and virulence of *Pseudomonas syringae* subsp. savastanoi. J. Bacteriol. **170:**2367–2373.
12. **Grant, S. R., E. J. Fisher, J. H. Chang, B. M. Mole, and J. L. Dangl.** 2006. Subterfuge and manipulation: type III effector proteins of phytopathogenic bacteria. Annu. Rev. Microbiol. **60:**425–449.
13. **Guttman, D. S., S. J. Gropp, R. L. Morgan, and P. W. Wang.** 2006. Diversifying selection drives the evolution of the type III secretion system pilus of *Pseudomonas syringae*. Mol. Biol. Evol. **23:**2342–2354.
14. **Heath, M. C.** 2000. Hypersensitive response-related death. Plant Mol. Biol. **44:**321–334.
15. **Herrero, M., V. de Lorenzo, and K. N. Timmis.** 1990. Transposon vectors containing non-antibiotic resistance selection markers for cloning and stable chromosomal insertion of foreign genes in gram-negative bacteria. J. Bacteriol. **172:**6557–6567.
16. **Hirano, S. S., and C. D. Upper.** 2000. Bacteria in the leaf ecosystem with emphasis on *Pseudomonas syringae*—a pathogen, ice nucleus, and epiphyte. Microbiol. Mol. Biol. Rev. **64:**624–653.
17. **Inoue, Y., and Y. Takikawa.** 2006. The *hrpZ* and *hrpA* genes are variable, and useful for grouping *Pseudomonas syringae* bacteria. J. Gen. Plant Pathol. **72:**26–33.
18. **Joardar, V., M. Lindeberg, R. W. Jackson, J. Selengut, R. Dodson, L. M. Brinkac, S. C. Daugherty, R. DeBoy, A. S. Durkin, M. G. Giglio, R. Madupu, W. C. Nelson, M. J. Rosovitz, S. Sullivan, J. Crabtree, T. Creasy, T. Davidsen, D. H. Haft, N. Zafar, L. W. Zhou, R. Halpin, T. Holley, H. Khouri, T. Feldblyum, O. White, C. M. Fraser, A. K. Chatterjee, S. Cartinhour, D. J. Schneider, J. Mansfield, A. Collmer, and C. R. Buell.** 2005. Whole-genome sequence analysis of *Pseudomonas syringae* pv. phaseolicola 1448A reveals divergence among pathovars in genes involved in virulence and transposition. J. Bacteriol. **187:**6488–6498.
19. **Kennelly, M. M., F. M. Cazorla, A. de Vicente, C. Ramos, and G. W. Sundin.** 2007. *Pseudomonas syringae* diseases of fruit trees: progress toward understanding and control. Plant Dis. **91:**4–17.
20. **Kuehn, M. J., and N. C. Kesty.** 2005. Bacterial outer membrane vesicles and the host-pathogen interaction. Genes Dev. **19:**2645–2655.
21. **McBroom, A. J., and M. J. Kuehn.** 2007. Release of outer membrane vesicles by gram-negative bacteria is a novel envelope stress response. Mol. Microbiol. **63:**545–558.
22. **McCann, M. C.** 1997. Tracheary element formation: building up to a dead end. Trends Plant Sci. **2:**333–338.
23. **Miller, J. H. (ed.).** 1972. Experiments in molecular genetics. Cold Spring Harbor Laboratory, Cold Spring Harbor, NY.
24. **Mittler, R., L. Simon, and E. Lam.** 1997. Pathogen-induced programmed cell death in tobacco. J. Cell Sci. **110:**1333–1344.
25. **Morel, J. B., and J. L. Dangl.** 1997. The hypersensitive response and the induction of cell death in plants. Cell Death Differ. **4:**671–683.
26. **Murillo, J., H. Shen, D. Gerhold, A. Sharma, D. A. Cooksey, and N. T. Keen.** 1994. Characterization of pPT23B, the plasmid involved in syringolide production by *Pseudomonas syringae* pv. tomato PT23. Plasmid **31:**275–287.
27. **Ortiz-Martín, I., A. P. Macho, L. Lambersten, C. Ramos, and C. R. Beuzón.** 2006. Suicide vectors for antibiotic marker exchange and rapid generation of multiple knockout mutants by allelic exchange in Gram-negative bacteria. J. Microbiol. Methods **67:**395–407.
28. **Penyalver, R., A. García, A. Ferrer, E. Bertolini, J. M. Quesada, C. I. Salcedo, J. Piquer, J. Pérez-Panadés, E. A. Carbonell, C. del Río, J. M. Caballero, and M. M. López.** 2006. Factors affecting *Pseudomonas savastanoi* pv. savastanoi plant inoculations and their use for evaluation of olive cultivar susceptibility. Phytopathology **96:**313–319.
29. **Pérez-Martínez, I., L. Rodríguez-Moreno, I. M. Matas, and C. Ramos.** 2007. Strain selection and improvement of gene transfer for genetic manipulation of *Pseudomonas savastanoi* isolated from olive knots. Res. Microbiol. **158:**60–69.
30. **Pérez-Martínez, I., Y. Zhao, J. Murillo, G. W. Sundin, and C. Ramos.** 2008. Global genomic analysis of *Pseudomonas savastanoi* pv. savastanoi plasmids. J. Bacteriol. **190:**625–635.
31. **Powell, G. K., and R. O. Morris.** 1986. Nucleotide sequence and expression of a *Pseudomonas savastanoi* cytokinin biosynthetic gene: homology with *Agrobacterium tumefaciens tmr* and *tzs* loci. Nucleic Acids Res. **14:**2555–2565.
32. **Rodríguez-Moreno, L., A. Barceló-Munoz, and C. Ramos.** 2008. In vitro analysis of the interaction of *Pseudomonas savastanoi* pvs. savastanoi and nerii with micropropagated olive plants. Phytopathology **98:**815–822.
33. **Rodríguez-Moreno, L., J. A. Jiménez, and C. Ramos.** 2009. Endopathogenic lifestyle of *Pseudomonas savastanoi* pv. savastanoi in olive knots. Microb. Biotechnol. **2:**476–488.
34. **Sambrook, J., and D. Russell.** 2001. Molecular cloning: a laboratory manual, 3rd ed. Cold Spring Harbor Laboratory Press, Cold Spring Harbor, NY.
35. **Sarkar, S. F., J. S. Gordon, G. B. Martin, and D. S. Guttman.** 2006. Comparative genomics of host-specific virulence in *Pseudomonas syringae*. Genetics **174:**1041–1056.
36. **Sarkar, S. F., and D. S. Guttman.** 2004. Evolution of the core genome of *Pseudomonas syringae*, a highly clonal, endemic plant pathogen. Appl. Environ. Microbiol. **70:**1999–2012.
37. **Simon, R., U. Priefer, and A. Puhler.** 1983. A broad host range mobilization system for *in vivo* genetic engineering: transposon mutagenesis in Gram-negative bacteria. Biotechnology **1:**784–791.
38. **Sisto, A., M. G. Cipriani, and M. Morea.** 2004. Knot formation caused by *Pseudomonas syringae* subsp. savastanoi on olive plants is *hrp*-dependent. Phytopathology **94:**484–489.
39. **Skorupski, K., and R. K. Taylor.** 1996. Positive selection vectors for allelic exchange. Gene **169:**47–52.
40. **Surico, G.** 1977. Histological observations on olive knots. Phytopathol. Mediterr. **16:**109–125.
41. **Surico, G., N. S. Iacobellis, and A. Sisto.** 1985. Studies on the role of indole-3-acetic acid and cytokinins in the formation of knots on olive and oleander plants by *Pseudomonas syringae* pv. savastanoi. Physiol. Plant Pathol. **26:**309–320.
42. **Taira, S., J. Tuimala, E. Roine, E. L. Nurmiaho-Lassila, H. Savilahti, and M. Romantschuk.** 1999. Mutational analysis of the *Pseudomonas syringae* pv. tomato *hrpA* gene encoding Hrp pilus subunit. Mol. Microbiol. **34:**737–744.
43. **Tamura, K., J. Dudley, M. Nei, and S. Kumar.** 2007. MEGA4: molecular evolutionary genetics analysis (MEGA) software version 4.0. Mol. Biol. Evol. **24:**1596–1599.
44. **Temsah, M., L. Hanna, and A. T. Saad.** 2008. Anatomical pathogenesis of *Pseudomonas savastanoi* on olive and genesis of knots. J. Plant Pathol. **90:**225–232.
45. **Thompson, J. D., T. J. Gibson, F. Plewniak, F. Jeanmougin, and D. G. Higgins.** 1997. The CLUSTAL_X Windows interface: flexible strategies for multiple sequence alignment aided by quality analysis tools. Nucleic Acids Res. **25:**4876–4882.
46. **Vasanthakumar, A., and P. S. McManus.** 2004. Indole-3-acetic acid-producing bacteria are associated with cranberry stem gall. Phytopathology **94:**1164–1171.
47. **Yap, M. N., J. D. Barak, and A. O. Charkowski.** 2004. Genomic diversity of *Erwinia carotovora* subsp. carotovora and its correlation with virulence. Appl. Environ. Microbiol. **70:**3013–3023.